TA15钛合金与 304不锈钢的电子束焊接

王 廷, 张秉刚, 陈国庆, 冯吉才
(哈尔滨工业大学 现代焊接生产技术国家重点实验室, 哈尔滨 150001)

摘 要: 对 TA15钛合金和 304不锈钢的电子束焊接进行了研究, 对接头显微组织、相组成和显微硬度进行了分析. 结果表明, TA15与 304不锈钢电子束焊接性较差, 在较小的热应力下即在焊缝内产生大量裂纹. 焊缝内生成连续分布的化合相, 主要包括 TiFe$_2$, TiFeCr$_2$T等, 脆性化合物的产生是裂纹形成的根本原因. 焊缝区内显微硬度明显高于母材, 且 TiFe$_2$的硬度高于 TiFe相, 贯穿裂纹在 TiFe$_2$相富集的区域产生. 二者的直接电子束焊接难以实现, 需要添加中间层以改善焊缝的冶金条件, 改变化合物的种类和分布, 从而实现可靠连接.

关键词: TA15钛合金; 304不锈钢; 电子束焊接; 显微组织; 显微硬度
中图分类号: TG456.3 文献标识码: A 文章编号: 0253-360X(2010)05-0053-04

王 廷

0 序 言

新一代航空发动机为了进一步增强其快捷机动性能, 要求提高发动机自身的推重比, 采用钛合金取代部分钢质体用于发动机推力室身部制造, 可实现局部减重, 满足新一代大推力火箭发动机的高性能需求[1].

钛合金和钢铁材料理化性能存在着巨大的差异, 表现在熔点、热膨胀系数、以及热导率差异, 同时钛与铁的互溶性差, 二者容易形成多种脆性的金属间化合物, 熔化焊时因接头的脆性以及较大的热应力而难以实现[2]. 采用压力焊和钎焊能够避免熔化焊时的问题, 实现可靠连接, 但零件尺寸和使用条件受到极大限制[3,4]. 李标峰[5]采用纯钛和纯铁对钛与钢的 TIG焊进行了研究, 结果表明钛—铁熔焊焊缝中存在着脆性的 TiFe, TiFe$_2$相及低熔点共晶组织, 是焊缝脆化的根本原因. 焊缝金属的最大硬度值在 740~1 324 HV范围.

电子束焊接具有能量密度高, 加热位置和加热半径精确可控的特点, 能够控制熔池尺寸及两种金属的熔合比, 在进行异种材料焊接时具有独特的优势[6]. 作者对 TA15钛合金和 304不锈钢的电子束焊接进行了研究, 分析了接头的显微组织、相组成和显微硬度, 为两种金属电子束焊接工艺的改进提供了试验依据.

收稿日期: 2009-05-21
基金项目: 中国航天联合技术创新资助项目

1 试验方法

试验所用钛合金为近 α型钛合金 TA15, 不锈钢为 304奥氏体不锈钢, 它们的化学成分如表 1和表 2所示, 物理性能参数如表 3所示[7,8]. 试验前将板材切割为 50 mm×3 mm×2.5 mm的条状, 对接面为 50 mm×2.5 mm侧面, 目的是尽量降低焊接时接头的横向应力, 便于研究影响二者焊接性的冶金因素.

表 1 TA15化学成分 (质量分数, %)
Table 1 Chemical composition of TA15

Al	Zr	Mo	V	杂质	Ti
5.5~7.0	1.5~2.5	0.5~2.0	0.8~2.5	≤0.7	余量

表 2 304不锈钢化学成分 (质量分数, %)
Table 2 Chemical composition of 304 stainless steel

C	Ni	Cr	Mn	Si	杂质	Fe
≤0.07	8~11	17~19	≤2.0	≤1.0	≤0.03	余量

表 3 TA15和 304物理性能参数
Table 3 Physical properties of TA15 and 304

材料	密度 ρ/(g·cm^{-3})	熔点温度 T_m/℃	比热容 c/(J·kg^{-1}·K^{-1})	热导率 λ/(W·m^{-1}·K^{-1})	线膨胀系数 α/(10^{-6}·K^{-1})
TA15	4.45	1 700	545	8.8	8.9
304	7.93	1 450	502	14.6	16.0

为了进一步降低焊接应力, 焊接时利用散焦电

子束进行了焊前预热和焊后后热, 散焦聚焦电流为 3 370 mA, 速度为 300 mm/min. 为防止开裂, 焊接时采用较小的束流, 较小的焊接速度. 工艺参数为: 加速电压 55 kV, 表面聚焦电流 2 450 mA, 束流 6 mA, 焊接速度 400 mm/min.

焊后沿垂直焊接方向截取金相试样, 采用 S4700扫描电子显微镜进行了显微组织观察和成分分析, 采用 D/max— rB旋转阳极 X射线衍射仪分析了接头的相组成. 采用 HV— 100型显微硬度计对接头横截面水平方向显微硬度分布进行了测量, 载荷为 1 N, 加载时间为 10 s.

2 试验结果与讨论

2.1 接头组织和成分分析

2.1.1 接头宏观形貌

图 1所示为焊缝横截面宏观形貌, 可以看出由于焊接束流较小, 未熔透整个厚度. 同时可以看出, 焊缝内部和两边界处都有裂纹产生, 说明焊缝内生成了大量的脆性相. 由于焊接过程中的热输入较小, 同时通过工艺设计减小了降温速率和温度梯度, 焊接过程中的热应力较小, 说明焊缝脆性较大, 在极小的应力作用下即可开裂. 裂纹在 304侧焊缝区内更密集, 且贯穿整个焊缝, 说明靠近 304侧的生成相脆性更大.

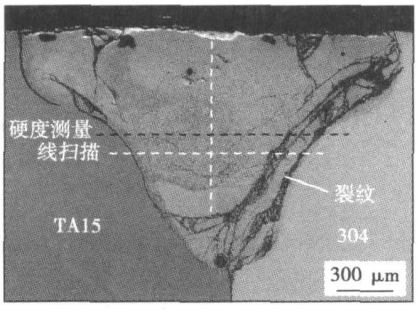

图 1 焊缝横截面宏观形貌

Fig. 1 Macrostructure of cross section of weld

2.1.2 主要元素在焊缝中的分布

焊缝中反应相的种类和形态取决于两种被焊金属中各组元在焊缝中的分布情况, 即跟二者的熔化量有关. 对焊缝横截面上各组元在水平方向和竖直方向的线分布进行了线扫描分析, 结果如图 2所示. 从图 2a中可以看出各组元在焊缝水平方向分布均匀, 只有在靠近两侧母材的焊缝区内有一定的梯度. 从图 2b中可以看出在竖直方向各组元成分也比较均匀, 只是焊缝底部 Fe元素含量略微高于顶部, 而 Ti元素含量则在顶部略高于底部. 这种分布说明两种金属熔化后, 在熔池内混合充分, 没有出现明显的偏析, 这为焊缝内反应相的均匀分布提供了条件. 同时由于密度的差异, 密度较大的液态铁倾向于在焊缝底部沉积, 密度较小的液态钛倾向于浮于焊缝顶部, 但由于熔池冷却速度快, 因此焊缝顶部与底部的成分差异并不大.

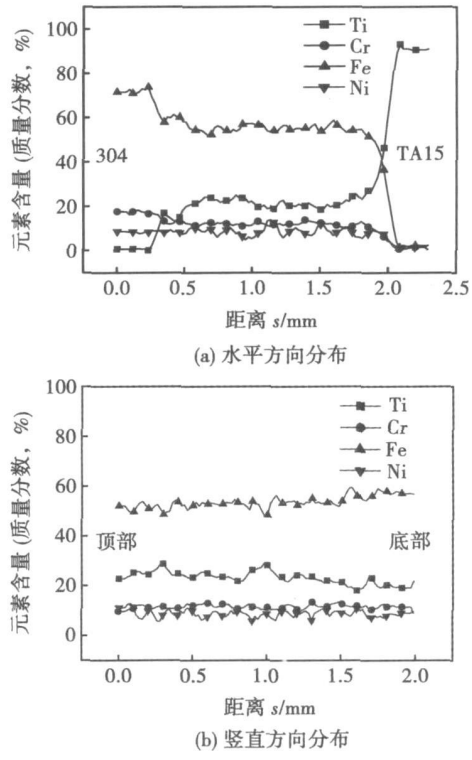

图 2 主要元素在焊缝中的分布

Fig. 2 Distribution in weld of main elements

2.1.3 显微组织及相分析

从上面的分析可知, 钛合金与不锈钢焊接时在焊缝区内产生大量裂纹, 以至于无法实现二者的连接, 因此重点对该区域的显微组织和相组成进行了分析. 根据裂纹的产生位置, 可以将焊缝分成三个区域, 即近钛侧焊缝区、焊缝中心区及近钢侧焊缝区. 图 3所示为近钛侧焊缝区显微组织形貌, 从图中可以看出, 该区域主要包括沿母材连续分布的 A相和细小的 B相. 裂纹沿 B相界面扩展. 对 A和 B分别进行了成分分析, 结果如表 4所示. 从表中可以看出, 两种相虽然形态不同, 但成分接近, 处于钛与 TiFe的共晶反应区, 为钛基固溶体与 TiFe化合物的共晶产物. 所不同的是 A相沿母材固相界面结晶, Ti元素含量略高. B相由于比较细小, 相界面多且脆, 所以裂纹在此处容易扩展.

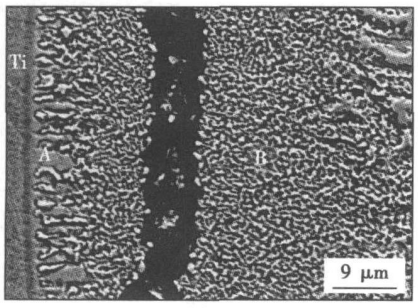

图 3　近钛侧焊缝区显微组织形貌

Fig. 3　Microstructure of weld near TA15 side

表 4　各相化学成分（原子分数，%）

Table 4　Chemical composition of each phase

	Ti	Al	Fe	Cr	Ni
A相	68	6	19	5	3
B相	59	6	22	3	10

图 4为焊缝中心的显微组织形貌，该区由两种相组成，分别为块状分布的 C相和鱼骨状的 D相，其中 C相以连续分布的 D相为界. 裂纹穿过两相内部扩展. 对 C相和 D相进行了成分分析，结果如表 5所示，可以看出该区为 TiFe2与 FeTi的共析反应区，C相为 TiFe2，Cr2Ti混合物，且以 TiFe2为主，D相为 FeTi.

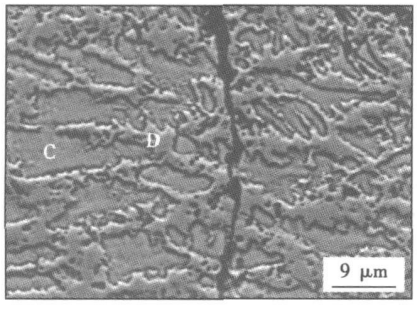

图 4　焊缝中心区显微组织形貌

Fig. 4　Microstructure of central weld

表 5　各相化学成分（原子分数，%）

Table 5　Chemical composition of each phase

	Ti	Al	Fe	Cr	Ni
C相	33	4	38	20	5
D相	43	6	31	9	11

图 5为近钢侧焊缝区显微组织形貌. 从图 5中可以看出该区域可以分为两部分，分别标记为 Ⅰ区和 Ⅱ区，其中 Ⅰ区由两种相 E和 F组成. 对 Ⅱ区进一步放大（图 6），可见该区为典型的共晶组织，共晶相分别标记为 H和 G相. 裂纹在 Ⅰ区内穿过 E相和 F相内部扩展.

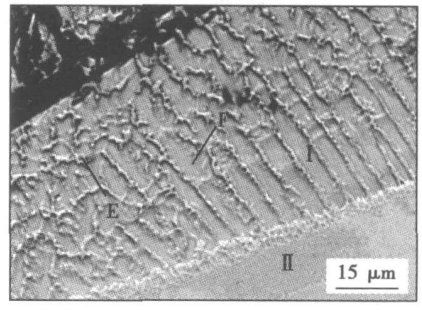

图 5　近钢侧焊缝区显微组织形貌

Fig. 5　Microstructure of weld near steel side

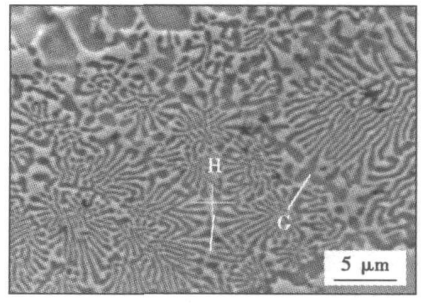

图 6　近钢侧焊缝区内共晶组织形貌

Fig. 6　Eutectic structure in weld near steel side

分别对 E相、F相、H相和 G相进行了成分分析，结果如表 6所示. 可以看出 E相与 D相，C相与 F相成分接近，说明该区与焊缝中心区在焊接过程中发生了类似的冶金反应. 不同的是该区内 TiFe2，Cr2Ti混合物与 FeTi的比例高于焊缝中心区. 由于裂纹在该处较集中且贯穿整个焊缝，说明 TiFe2相的脆性大于 FeTi相. G相和 H相为铁与 TiFe2的共晶产物，其中 G相为 TiFe2，H为铁基固溶体.

表 6　各相化学成分（原子分数，%）

Table 6　Chemical composition of each phase

	Ti	Al	Fe	Cr	Ni
E相	35	6	37	9	13
F相	34	6	44	12	4
G相	19	2	54	13	12
H相	9	3	58	18	12

由于该区内产生了贯穿裂纹，对裂纹表面进行了 XRD分析，结果如图 7所示. 衍射分析结果证明了上述分析中各可能相的存在. 同时也表明，贯穿

裂纹产生于以 Fe_2Ti为主的混合有 FeTi,Cr_2Ti等化合物的区域,说明大量脆性化合物的生成是焊接性较差的主要原因.

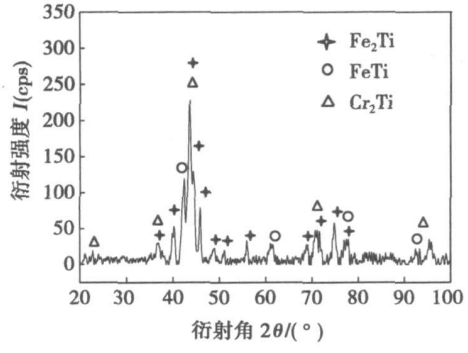

图 7 近钢侧焊缝区内贯穿裂纹表面 XRD图谱

Fig. 7 XRD pattern of crack surface in weld near steel side

2.2 显微硬度分析

为了进一步分析接头中不同化合物脆性,对接头横截面水平方向的显微硬度进行了测量,结果如图 8所示. 从图 8中可以看出焊缝区显微硬度显著高于两侧母材,硬度在 700~1 200 HV之间,说明焊缝生成的化合物塑性较差,故在极小的热应力作用下即发生脆性开裂. 从图中还可以发现,钛侧至钢侧,显微硬度值先增大后减小. 在距离钢侧熔合线约 200 μm处达到最大,贯穿裂纹在此处产生. 显微硬度的这种分布与元素及相组成有一定的对应关系,近钛侧焊缝区内 Ti元素含量较高,该位置的相组成为钛与 $TiFe_2$的共晶体,硬度较低;靠近钢侧焊缝区内 Ti元素含量降低,Fe元素含量升高,相组成为以 $TiFe_2$为主的各种化合物的混合物,此处硬度值达到最高水平;而在最靠近钢侧界面的焊缝区内为铁基固溶体与 $TiFe_2$的共晶组织,故硬度明显降低. 显微硬度的这种分布也说明了大量化合物的生成是 TA15与 304不锈钢电子束焊接性较差的根本原因,而且 $TiFe_2$的脆性大于 FeTi化合物.

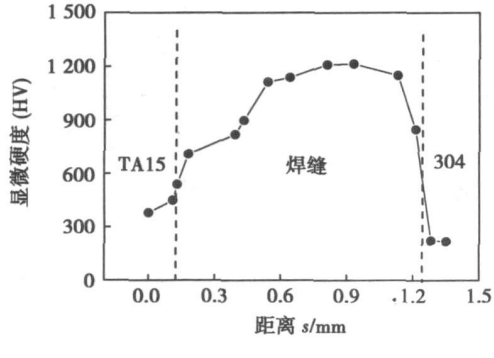

图 8 焊缝横截面显微硬度分布

Fig. 8 Microhardness distribution in cross section of weld

3 结 论

(1) TA15与 304不锈钢电子束焊接性较差,在较小的热应力下即在焊缝内产生大量裂纹,无法实现连接.

(2) 焊缝内生成连续分布的化合相,主要包括 $TiFe_2$, TiFe, Cr_2Ti等. 这些化合物的产生是裂纹形成的根本原因.

(3) 焊缝区内显微硬度明显高于母材,且 $TiFe_2$的硬度高于 TiFe相,贯穿裂纹在 $TiFe_2$相富集的区域产生.

(4) 二者的直接熔化焊接难以进行,需要添加中间层以改善焊缝的冶金条件,改变化合物的种类和分布.

参考文献:

[1] Özdemir N, Bilgin B. Interfacial properties of diffusion bonded Ti-6Al-4V to 304 stainless steel by inserting a Cu interlayer[J]. International Journal of Advanced Manufacturing Technology, 2009, 41(5-6): 519-526.

[2] 孙荣禄, 张九海. 钛及钛合金与钢焊接的问题及研究现状[J]. 宇航材料工艺, 1997(2): 7-11.
Sun Ronglu, Zhang Jiuhai. Welding problems and present situation of titanium or titanium alloy and steel[J]. Aerospace Meterials & Technology, 1997(2): 7-11.

[3] Yue X, He P, Feng J C, et al. Microstructure and interfacial reactions of vacuum brazing titanium alloy to stainless steel using an AgCuTi filler metal[J]. Materials Characterization, 2008, 59(12): 1721-1727.

[4] Ghosh M, Bhanumurthy K, Kale G B, et al. Diffusion bonding of titanium to 304 stainless steel[J]. Journal of Nuclear Materials, 2003, 322(2-3): 235-241.

[5] 李标峰. 钛与钢及钛复合钢板的焊接性研究(I)[J]. 材料开发与应用, 2004, 19(1): 41-44.
Li Biaofeng. Study on the weldability of Titanium and steel and titanium clad steel plate(I)[J]. Development and Application of Materials, 2004, 19(1): 41-44.

[6] Sun Z, Karppi R. The application of electron beam welding for the joining of dissimilar metals: an overview[J]. Journal of Materials Processing Technology, 1996, 59(3): 257-267.

[7] 黄伯云, 李成功, 石力开, 等. 中国材料工程大典第 4卷[M]. 北京: 化学工业出版社, 2006.

[8] 干 勇, 田志凌, 董 瀚, 等. 中国材料工程大典第 2卷[M]. 北京: 化学工业出版社, 2006.

作者简介: 王 廷, 男, 1984年出生, 博士研究生. 研究方向为新材料及异种材料的连接. 发表论文 10篇.
Email: fgwangting@163.com

proach for the sub-system of plasma jet generation was presented in this paper based on the rule sets supervision and multi-model adaptive control system structure.

Key words: plasma spraying; plasma jet morphology; intelligent control; data mining; clustering analysis

Brazing of aluminum matrix composites SiC_p/ZL101 to Kovar alloy 4J29 NIU Jitai[1,2], LU Jinbin[1], MU Yunchao[1], LUO Xiangwei[3] (1. Department of Materials and Chemical Engineering, Zhongyuan University of Technology, Zhengzhou 450007, China; 2. State Key Laboratory of Advanced Welding Production Technology, Harbin Institute of Technology, Harbin 150001, China; 3. Department of Materials Science & Engineering, Zhengzhou University, Zhengzhou 450002, China). p 37 - 40

Abstract: SiC_p/ZL101 composites containing 55% SiC_p and Kovar alloy 4J29 were chosen as base metals. After being electroplated by Ni on the SiC_p/ZL101, the two materials were brazed by Zn-Cd-Ag as filler metal at the 420 ℃ for 7 min. Moreover, the interfacial microstructures and fracture appearances were investigated by SEM and EDS. The results show that the electroplated Ni on the surface of SiC_p/ZL101 can improve the filler's wettability to the composite material. There are transition layers not only between the filler and Kovar alloy, but also between the filler and the electroplated Ni layer, which shows the filler metal, the electroplated Ni layer, the composites and Kovar alloy can realize metallurgically joining by diffusion. The fracture analysis shows that the fracture happens inside the composites near the electroplated Ni layer.

Key words: aluminum matrix composites; Kovar alloy; brazing Ni electroplating

Analysis of chemical reaction on weld pool surface in activating TIG welding of aluminum alloys HUANG Yong, FAN Ding, SHAO Feng (State Key Laboratory of New Non-ferrous Metal Materials, Lanzhou University of Technology, Lanzhou 730050, China). p 41 - 44

Abstract: For activating TIG welding of aluminum alloys, including A-TIG welding, FB-TIG welding and FZ-TIG welding, the analysis of chemical reaction between the activating fluxes and the weld pool metal has great significance to certain the feasibility of these welding processes and instruct the developments of activating fluxes. Through the XRD analysis of weld surface slag, the chemical reaction thermodynamics was calculated based on functional determinant of Gibbs' Free Energy, and the chemical reaction on welding pool was analyzed. It is found that, for the FZ-TIG welding, with multi-component flux FZ108 developed by authors as central region flux and SiO_2 as outer region flux, the endothermic reactions between flux FZ108 and the welding pool metal can constrict the arc and increase weld penetration. For the A-TIG welding with flux FZ108, the few absorbed heat or the released heat of the chemical reactions has small influence on the arc. For the FB-TIG welding with flux SiO_2, the chemical reaction between the flux and the weld pool metal and its surface oxide film does not happen, and the arc is not affected through these chemical reactions.

Key words: aluminum alloy; A-TIG welding; activating flux; chemical reaction; arc constriction

Microstructures and mechanical properties of transient liquid phase bonded Ti_3Al based alloy joints GU Xiaoyan[1], SUN Daqian[1], REN Zhen'an[1], LIU Li[2], DUAN Zhenzhen[2] (1. Key Laboratory of Automobile Materials, Jilin University, Changchun 130025, China; 2. Changchun Railway Vehicles Co., LTD., Changchun 130062, China). p 45 - 48

Abstract: Microstructure and mechanical properties of Ti_3Al based alloy joints bonded by transient liquid phase bonding were studied by scanning electron microscope (SEM), energy dispersive X-ray spectroscope (EDS), X-ray diffraction (XRD) and universal test machine. The results show that the integrated joints were prepared by TLP bonding with the TiZrNiCu alloy interlayer. The high bonding temperature and long bonding time help to obtain the joints with uniform composition and microstructure. With bonding temperature and bonding time increasing, the width of the bonding zone increases and reaction zones decreases. When bonding time is 60 min at bonding temperature of 900 ℃, the joint microstructure consists of Ti solid solution, Ti_3Al and Ti_2Cu and the joint strength of 420 MPa can be obtained.

Key words: Ti_3Al based alloy; transient liquid phase diffusion bonding; microstructure; shear strength

CoNiCrAlY alloy deposited on surface of SCH13 steel by laser cladding ZHANG Song[1], WANG Mingsheng[1], ZHANG Kaixiang[1], ZHANG Chunhua[1], YAN Yonggen[2] (1. School of Materials Science and Engineering, Shenyang University of Technology, Shenyang 110023, China; 2. Baoshan Iron & Steel Co., Ltd., Shanghai 201900, China). p 49 - 52

Abstract: The surface of SCH113 steel was deposited with CoNiCrAlY alloy by a high power CO_2 laser. Through, the excellent coatings can be acquired by the optimized process parameters. The micro-structure, composition, hardness and corrosive resistance of the coating were examined by scanning electron microscope (including EDS microanalysis), X-ray diffraetometry, micro thickness meter, wear test machine. The results indicated that the coating of CoNiCrAlY alloy has a good metallurgical combination with SCH13 steel, and the other characteristics such as fine microstructure, no cracks, low dilution rate and the smooth transition of elements at the interface. The coatings were consisted of γ-Co, $FeCr_{0.29}Ni_{0.16}C_{0.06}$, FeNi, CoC_x and $Cr_{23}C_6$ phases. The average microhardness of the coating is 3 times higher than that of the SCH13 steel. Furthermore, the wear resistance of laser cladded coating is 3.42 times higher than that of the matrix.

Key words: SCH13 steel; laser cladding; CoNiCrAlY alloy coatings; microstructure; property

Electron beam welding of TA15 titanium alloy to 304 stainless steel WANG Ting, ZHANG Binggang, CHEN Guoqing, FENG Jicai (State Key Laboratory of Advanced Welding Production Technology, Harbin Institute of Technology, Harbin 150001, China). p 53 - 56

Abstract: Electron beam welding experiment of TA15 titanium alloy to 304 stainless steel was carried out. Microstructure and micro-hardness distribution of joint were examined. The results showed that the weldability of electron beam welding of TA15 titanium alloy to 304 stainless steel was so poor that many

cracks in the whole weld zone were produced. The weld zone was characterized by a large amount of continuously distributed compounds such as $TiFe_2$, TiFe and Cr_2Ti. The formation of these kinds of brittle compounds was the main reason of the cracks. The micro-hardness in weld zone was much higher than that in base metal. And $TiFe_2$ phase was harder than TiFe phase, so the throughout crack was found in the $TiFe_2$-rich zone. Direct electron beam welding of these two alloys was hardly completed. Some interlayer alloys have to be used to improve the metallurgical condition and change the kind and distribution of the compounds.

Key words: TA15 titanium alloy; 304 stainless steel; electron beam welding; microstructure; micro-hardness

Analysis on vacuum brazing of CBN grits with Ti-base filler

LU Jinbin[1,2], MU Yunchao[1,2], MENG Pu[1] (1. Department of Materials and Chemical Engineering, Zhongyuan University of Technology, Zhengzhou 450007, China; 2. Henan Engineering Laboratory of High-quality Superhard Materials Tools, Zhongyuan University of Technology, Zhengzhou 450007, China). p 57 - 60

Abstract: Ti-Zr-Ni-Cu filler was utilized to braze CBN grits in vacuum furnace at different temperatures and times, and good bonding between CBN and steel substrate was gotten. The microstructure and the element distribution of the bonding interface, as well as the topography and the phase structure of the compounds on the surface of brazed CBN grits were analyzed by SEM, EDS and XRD. The results show that a layer of needle-like, or block-like Ti compounds such as TiB_2 and TiN are formed on the surface of the CBN, thus CBN grits and Ti-Zr-Ni-Cu filler realize chemical metallurgic joining in the interface. And the analysis on fracture appearance shows that the fracture between CBN and Ti-Zr-Ni-Cu filler occurs in CBN, so it can be considered that the joining strength between CBN and Ti-Zr-Ni-Cu filler is higher than that of the CBN.

Key words: vacuum brazing; Ti-base filler; cubic boron nitride

Microstructure of Be/Al/Be joint by welded laser beam

LI Yubin, MENG Daqiao, LIU Kezhao, XIE Zhiqiang (China Academy of Engineering Physics, Mianyang 621907, Sichuan, China). p 61 - 64

Abstract: Application of beryllium alloy was joined with laser welding by taking aluminum as transition material. The microstructure and properties of the welded joint were studied by means of scanning electron microscope (SEM), optical microscope (OM), and X ray diffraction apparatus (XRD). The results indicated that the microstructure was composed of quasi-composite compound phase formed by beryllium and aluminum. The shear strength lies between aluminum and beryllium. With percent of beryllium in weld zone being more, the size of beryllium and beryllium particle distribution change, the shear strength of welded joint is higher, the fracture mechanism is transformed form ductile fracture with fractographs of dimples to brittle fracture with quasi-cleavage feature. The intermetallic compound in weld zone is the main cause of fracture for Be/Al/Be laser welded joint.

Key words: beryllium; laser welding; microstructure; shear strength; fracture appearance

Effect of electrode force on welding quality of sheet to tube by single sided spot welding

LIANG Caiping, LIU Xiaohang, TIAN Haobin (Mechanics & Electronic Engineering Faculty, Shanghai Second Polytechnic University, Shanghai 201209, China). p 65 - 68

Abstract: Based on the structure characteristics of sheet to tube joined by spot welding, a welding system with servo gun was established. Due to large deformation of the weldments during the sheet to tube welding stage and unreliable ring nugget after welding, a new method was investigated to increase the weld quality based on the electrode force change. The effects of variable electrode force on weld tensile-shear strength and weld deformation were researched. The results show that the weld strength can be increased and weld deformation can be decreased by adjusting the electrode force in welding process. Comparatively, the change of electrode force during holding stage has less influence on weld quality. The studies can contribute to develop welding parameters for sheet to tube joining and to promote the wider application of single sided spot welding in the assembly of auto body.

Key words: single-sided resistance spot welding; servo gun; variable electrode force; welding quality

DSP based digital pulsed CO_2 welding power supply with sloping output characteristics

YU Jianrong, JIANG Lipei, ZOU Yong, GONG Yongfei (Beijing Institute of Petrochemical Technology, Beijing 102617, China). p 69 - 72

Abstract: A digital pulsed CO_2 welding power supply with sloping output characteristics based on digital signal processing controller was developed. It can automatically regulate the slope of external characteristic curves with predominant sloping characteristic algorithm in the welding process, and implement the stability of welding arc in wide field. In this system, the average arc voltage is preset in accordance with the feeding rate of a separate wire feeder, while full-bridge inverted main circuitry can be adopted independently. The digital pulse width modulation signals are generated directly at low hardware expense, and the control strategy is implemented through software. Furthermore, the needed slope rate of output characteristics is calculated with the software, the control signal is created and converted to dual-edge pulse output signal, and the arc voltage is automatically adjusted to maintain a stable arc. The simplified configuration shows high reliability, and the control program can also be updated by means of the upgrade interface for property enhancement. Welding test showed that the pulsed power supply with the sloping output characteristics has high stability and reliability.

Key words: pulsed CO_2 welding; sloping output characteristics; inverted power supply

Effect of flow rate and arc length changes on velocity and temperature field of TIG arc

DU Huayun[1], AN Yanli[1], WEI Yinghui[1], WANG Wenxian[1], FAN Ding[2] (1. College of Materials Science and Engineering, Taiyuan University of Technology, Taiyuan 030024, China; 2. College of Materials Science and Engineering, Lanzhou University of Technology, Lanzhou 730050, China). p 73 - 76

Abstract: A steady two-dimensional (2D) axisymmetric